Low-Cost, High-Sensitivity Hydrophone Based on Resonant Air Cavity

Huang Xinjing, Li Zan, Li Jian, Wang Xin, Feng Hao, Zhang Yu, and Rui Xiaobo

***Abstract*—Underwater acoustic ranging and detection usually require hydrophones to have high sensitivity at narrowband operating frequencies. Different from traditional sensitization methods with the help of new materials and solid/liquid resonance structure, this paper proposes a low-cost, high-sensitivity hydrophone based on a resonant air cavity containing an affordable MEMS microphone inside to sense the focused acoustic waves transmitted from the external water across the solid shell into the air cavity. Both finite element simulations and experiments are carried out to test its acoustic sensing performances. Resonance frequency and directivity of the proposed hydrophone are determined by the air cavity size and the acoustic mode, but is independent of the solid shell, which facilitates the precise designability. The sensitivity of the developed hydrophone at the resonance frequency is up to −157 dB re 1V/μPa calibrated by commercial standard hydrophone TC4013. Finally, several further considerations, improvements and applications on the proposed hydrophone are discussed.**

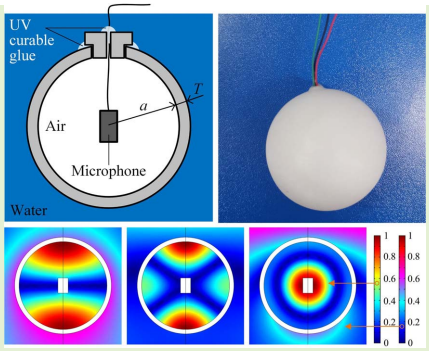

***Index Terms*— Acoustic sensor, hydrophone, resonant air cavity.**

I. Introduction

HYDROPHONES can transform underwater acoustic signals into electrical signals, and are widely used in underwater acoustic detection, ranging, communication, leak detection of liquid-filled pressurized pipelines, and so on [1]–[4]. Sensitivity is one of the most important performance indicators of a hydrophone. Higher sensitivity can bring higher signal-to-noise ratio (SNR) as well as longer detection and communication distance. To improve the sensitivity of hydrophones, on one hand, new materials with higher piezoelectric coefficients have been used to improve the piezoelectric conversion efficiency [5]–[7]; on the other hand, sensitization structures have been used to improve the coupling efficiency from the acoustic pressure to the vibration of the piezoelectric material for piezoelectric hydrophones [1] or to the dynamic strain of the optic fiber for optic-fiber based hydrophones [8]–[10].

Manuscript received December 15, 2020; accepted December 23, 2020. Date of publication December 29, 2020; date of current version February 17, 2021. This work was supported by the National Natural Science Foundation of China under Grant 61803280 and Grant 61973227. The associate editor coordinating the review of this article and approving it for publication was Prof. Stefan J. Rupitsch. *(Corresponding author: Li Jian.)*

The authors are with the State Key Laboratory of Precision Measuring Technology and Instruments, Tianjin University, Tianjin 300072, China, and also with the Binhai International Advanced Structural Integrity Research Centre, Tianjin 300072, China (e-mail: tjupipe@tju.edu.cn).

Digital Object Identifier 10.1109/JSEN.2020.3048066

When a hydrophone works in a frequency band far from the resonance frequency, its frequency response is flat and it can receive signals in a very wide frequency range. Nevertheless, some hydrophones for echo detection and communication usually work at resonance frequencies in order to obtain sufficiently high sensitivity, whereas at other frequencies their sensitivities are as low as possible to suppress the interference of environmental noises. For such kind of hydrophones used in narrow-band scenarios, many studies have been carried out to enhance the sensitivity by using sensitization structures with resonance phenomena.

There are two kinds of sensitization structures: (1) solid resonance structure whose resonance frequency is mainly determined by the shape, size and material properties of the solid structure; (2) liquid resonance cavity whose resonance frequency is mainly determined by the shape and size of the liquid cavity. Teng used thin piezoelectric spherical shell as the sensitization structure that is encapsulated in a polyurethane layer; thinner shell of the hollow sphere results in higher sensitivity [11]. Sadeghpour presented an omni-directional ultrasound transducer based on the vibration of two hemispherical shells working at the first-order resonance mode to efficiently transmit and receive underwater ultrasonic waves, and proved that its resonance frequency was directly related to the shell thickness [12]. For PZT-ring transducer working at electromechanical resonance, Wang employed a supermagnetostrictive rod to magnetically adjust and track the resonance frequency with a DC bias magnetic field in

order to maintain a high sensitivity [13]. Yang developed a new 1-3 piezoelectric composite hydrophone and proposed a dynamic model to sufficiently analyze the electromechanical response over the entire frequency range, especially around the resonance frequency where the sensitivity of weak signal detection is significantly enhanced [14].

People have also tried to add some ingenious structures that can transfer water sound pressure into vibration or dynamic strain of the sensing optical fiber, thus forming a hydrophone. Dass developed an optical fiber microtip based hydrophone consisting of an extrinsic Fabry-Perot interferometer, which detects acoustic signals by tracking the interference peaks or dips [15]. Peng developed an optical fiber vector hydrophone consisting of a rigid tube, a cylindrical mandrel, a metal case and two optical fiber coils, and the underwater acoustic pressure is reflected in the phase variance of the optical signal [16]. Chen proposed a compact fiber-optic hydrophone using a microknot resonator which is highly sensitive to cavity deformation caused by acoustic waves [17]. Ji designed a dumbbell-shaped ciliary MEMS vector hydrophone, which relies on the ciliary structure to sense the acoustic wave underwater [18]. However, almost all the hydrophones based on optical fibers require SLDs, circulators, tunable filters or FBG interrogators, and these discrete accessory devices cannot yet be integrated in a single small device, which makes the entire underwater acoustic sensing system large and complicated.

Besides solid resonance structure, liquid resonance cavity inside a solid shell has also been used to improve the hydrophone sensitivity. Li proposed a piezoelectric hydrophone with high receiving sensitivity near the resonant frequency based on a resonant liquid cavity inside the PZT tube; the acoustic pressure can be amplified by the liquid cavity via resonance and effectively coupled into the PZT tube [19]. Wang employed a Helmholtz resonator to improve the sensitivity of a conventional hydrophone; a solid shell with one end open formed the Helmholtz resonator to amplify the acoustic pressure which was then sensed by the conventional hydrophone inside the shell [20]. The effect of the wall thickness of the Helmholtz resonator on the resonance frequency becomes smaller as the thickness increases; finally, the resonance frequency approaches a constant and is no longer affected by the wall thickness [21]. Cylindrical Helmholtz resonator was also used for optic-fiber hydrophones as a mechanical anti-aliasing filter; the hydrophone has good acoustic low-pass filtering and is insensitive to hydrostatic pressure [22].

Different from the two types of resonance-based hydrophones above, this paper presents a new type of resonant air cavity hydrophone. It uses neither the resonance of a solid structure nor the resonance of a liquid cavity, but the resonance of a closed air cavity. An affordable MEMS microphone is sealed in the closed air cavity to sense the acoustic waves transmitted from the external water into the air cavity; the whole setup is inside water, and the hydrophone is made out of a MEMS microphone sealed inside an air cavity. Compared with other conventional hydrophones, the cost of the proposed one is very low and its fabrication is very simple, but its sensitivity and SNR (signal-to-noise ratio) at the resonance frequency are both very high. It can be used for underwater communication, underwater ranging, liquid-filled pipeline leak detection, etc. Working principle and design of the proposed hydrophone are described in Section II. Its acoustic sensing performance tests through simulations and experiments are illustrated in Section III. Several further considerations, improvements and applications on the proposed hydrophone are discussed in Section IV. Finally, Section V concludes the paper.

II. Hydrophone Design

The proposed hydrophone contains a solid shell forming an air cavity and a MEMS microphone that is enclosed in the cavity to sense the acoustic waves transmitted from the external water across the shell into the air cavity. MEMS microphones have advantages of ultra-small-size, lightweight, low-power, low-cost, less variation in sensitivity over temperatures and have better performance than normal-sized microphones, thus are perfect for various applications and small products [23]. They can be divided into different types by their transduction mechanisms: piezoelectric, piezoresistive, capacitive and optical [24]. The MEMS microphone adopted in this design is a widely used and relatively low-cost model that is based on mature capacitive technology. In addition, as for fiber-optic microphones, their sensing heads are also very small in size, and they can also be placed in a resonant cavity [25]–[27]. However, their supporting equipment are too complex, expensive, and huge. Currently, fiber-optic microphone system cannot be integrated into a chip, so MEMS instead of fiber-optic microphones are adopted by the proposed air resonant cavity hydrophone.

Sectional view and photo of the fabricated hydrophone are shown in Fig. 1. To maintain the air cavity, first the microphone is adhered to the T plug by the upper UV glue in the middle; second, the T plug is adhered to the spherical shell by the lower UV glue in the circum. Underwater sound can cause the shell to vibrate and the shell vibration can stimulate the air in the cavity to vibrate, thereby generating air acoustic waves. Because the density and elastic modulus of the solid and the density and bulk modulus of the water are much higher than that of the air, even if only a small part of the underwater acoustic energy is coupled into the air cavity, it will still produce considerable acoustic pressure in air. In addition, the solid shell provides a hard acoustic boundary to the air cavity so that acoustic resonances with different modes can occur in the air cavity. Each resonance has its own unique characteristic frequency and acoustic field distribution that can focus most of the acoustic energy into one or several small areas forming acoustic spot(s). A tiny MEMS microphone can be located at the acoustic spot to sense the amplified sound pressure without destroying the acoustic field distribution mode.

Denote the radius of the air cavity as a, and select the center of the sphere as the origin of the coordinate system. The inner wall is treated as a hard boundary with regards to the air inside.

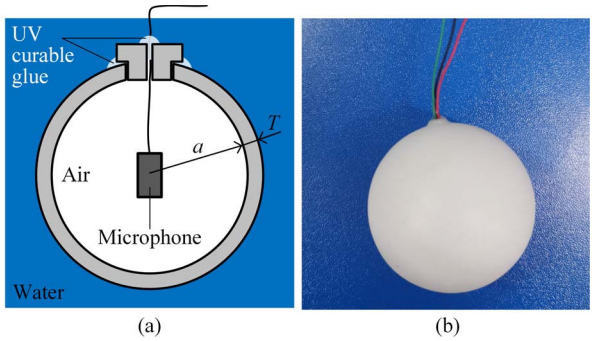

Fig. 1. Structure schematic (a) and photo (b) of the proposed hydrophone with an air cavity and a MEMS microphone inside.

In the r-θ-φ spherical coordinate system, the acoustic field equation can be expressed as follows:[28]

$$\left[\frac{1}{r^2}\frac{\partial}{\partial r}\left(r^2\frac{\partial}{\partial r}\right)+\frac{1}{r^2\sin\theta}\frac{\partial}{\partial\theta}\left(\sin\theta\frac{\partial}{\partial\theta}\right)+\frac{1}{r^2\sin^2\theta}\frac{\partial^2}{\partial\varphi^2}\right]\psi_\lambda + \left(\frac{\omega_\lambda}{c_0}\right)^2\psi_\lambda = 0, \quad (1)$$

with the boundary condition

$$\left.\frac{\partial\psi_\lambda}{\partial r}\right|_{r=a} = 0, \quad (2)$$

where ψ_λ is the normal mode of the acoustic pressure, ω_λ is the normal frequency, and c_0 is the acoustic velocity of the air inside the spherical cavity. The solution of (1) can be expressed as

$$\psi(r,\theta,\varphi,\omega_\lambda) = \left[A_l j_l\left(\frac{\omega_\lambda}{c_0}r\right) + B_l n_l\left(\frac{\omega_\lambda}{c_0}r\right)\right]Y_{lm}(\theta,\varphi), \quad (3)$$

where j_l and n_l are Bessel functions of the first and the second types, respectively. Because when $r = 0$, $n_l(0) \to \infty$, so that $B_l \equiv 0$, Equation (2) can be rewritten as follows:

$$j_l'\left(\frac{\omega_\lambda}{c_0}a\right) = 0. \quad (4)$$

The normal frequency is determined by the spherical Bessel function equation and is independent of m. Let x_{ql} be the qth root of the equation $j_l'(x) = 0$, then the normal frequency $\omega_\lambda = \omega_{ql}$ can be expressed as

$$\omega_{nl} = \frac{c_0 x_{ql}}{a} \quad (q = 0, 1, 2, \ldots, l = 0, 1, 2, 3, \ldots). \quad (5)$$

Therefore, when considering the acoustic field mode of the air cavity solely, the resonance frequencies of each mode are inversely proportional to the radius of the air cavity. In order to verify this relationship, a two-dimensional axisymmetric sound-structure coupling model is established for frequency domain simulation, as shown in Fig. 2(a)-(b). The exterior of the spherical shell is water, and the interior is air. The material of the spherical shell is photosensitive resin, which is the same as that used in hydrophone fabrication and subsequent experiments. The upper boundary is set as a plane radiation wave, and the bottom and right sides are set as perfectly

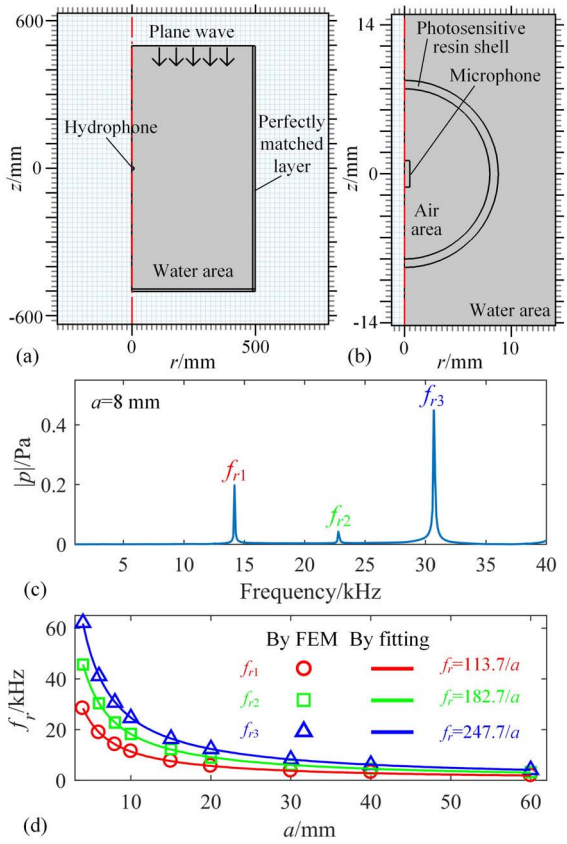

Fig. 2. Sound-structure coupling simulations in frequency domain: (a)-(b) simulation model; (c) frequency response of the hydrophone with $a = 8$ mm and $T = 0.8$ mm; (d) relationship between a and resonance frequencies of different orders.

matched layers to eliminate reflections. The frequency of the radiated acoustic waves is swept in the range of 1-40 kHz with a step of 200 Hz. Measurement point of the acoustic pressure is set near the microphone in the air cavity. Taking a hydrophone with $a = 8$ mm and $T = 0.8$ mm as an example, its frequency response curve obtained by simulation is shown in Fig. 2(c), and has three characteristic peaks appearing at 14200 Hz, 22800 Hz, and 30800 Hz. The radius a is swept to obtain the relationship between the resonance frequencies of first three orders and the cavity radius. As shown in Fig. 2(d), the two have an inverse relationship, which is consistent with the analysis above.

Since resonance may occur in both the spherical shell and the internal air cavity of the hydrophone, it is necessary to reveal where the resonance comes from, so as to rationally design the structure size of the hydrophone and obtain the desired resonance frequency. Therefore, three finite element simulations were carried out: (1) a spherical shell with $T = 0.8$ mm and $a = 8$ mm by using the solid mechanics module, modal analysis, where the resonant frequency is denoted as f_{rB}; (2) an air cavity with a radius of $a = 8$ mm using the pressure acoustics module, modal analysis, where the resonant frequency is denoted as f_{rC}; (3) the hydrophone with the same size immersed in water by using the acoustic-solid coupling module in frequency domain, and frequency sweeping simulations were carried out to compare with the results of the two

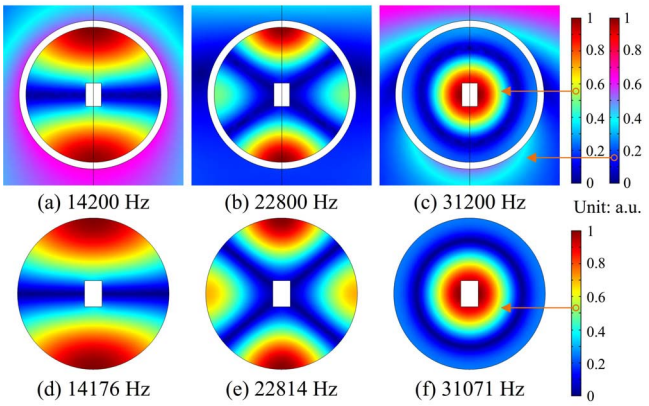

Fig. 3. Acoustic pressure distributions of the hydrophone and the ideal air cavity: (a)-(c) obtained by the sound-structure coupling simulation in frequency domain; (d)-(f) obtained by the modal analysis simulation.

TABLE I
COMPARISON OF THE RESONANT FREQUENCIES f_{rA}, f_{rB}, f_{rC} OF THE HYDROPHONE, AND ITS SHELL AND AIR CAVITY

Order of f_r	f_{rA} / Hz	f_{rB} / Hz	$(f_{rB}-f_{rA})/f_{rA}$	f_{rC} / Hz	$(f_{rC}-f_{rA})/f_{rA}$
1st	14200	17909	26%	14176	0.16%
2nd	22800	22057	3.6%	22814	0.06%
3rd	31200	35357	13.3%	31071	0.4%

modal analysis simulations, where the resonant frequency is denoted as f_{rA}.

The first several characteristic/resonance frequencies of the shell and the cavity were collected by the two modal analysis simulations, respectively. The resonance frequencies of the hydrophone were obtained by the acoustic-solid coupling module in frequency domain with frequency being swept. Three groups of resonance frequencies are listed together for comparison, as shown in Table I. The resonance frequencies of the hydrophone are very close to those of the air cavity, but have a large deviation from those of the spherical shell. The acoustic field distributions of the hydrophone at the resonance frequencies are almost identical to the modal analysis results of the air cavity, as shown in Fig. 3. Therefore, it can be concluded that the air cavity is the decisive factor affecting the resonance frequency of the proposed hydrophone, and the influence of the spherical shell on the resonance frequency can be negligible.

III. HYDROPHONE PERFORMANCE TESTS

The performance test apparatus for the proposed hydrophone is shown in Fig. 4. The experiment was performed in a glass water tank with the dimension of 1.4 m × 1.4 m × 1.4 m. The computer controlled the data acquisition card (NI USB-6366, 16-bit ADC resolution & 2 MS/s maximum sample rate) to generate an excitation signal with ten cycles, which was amplified by the power amplifier and then sent into the transmitting transducer (DYW-H08-1000, working frequency range of 1-40 kHz with two peaks at 8 kHz & 30 kHz). The pulses are 1071 mm and 500 mm long when the frequency is 14 kHz and 30 kHz respectively. The source level used is about

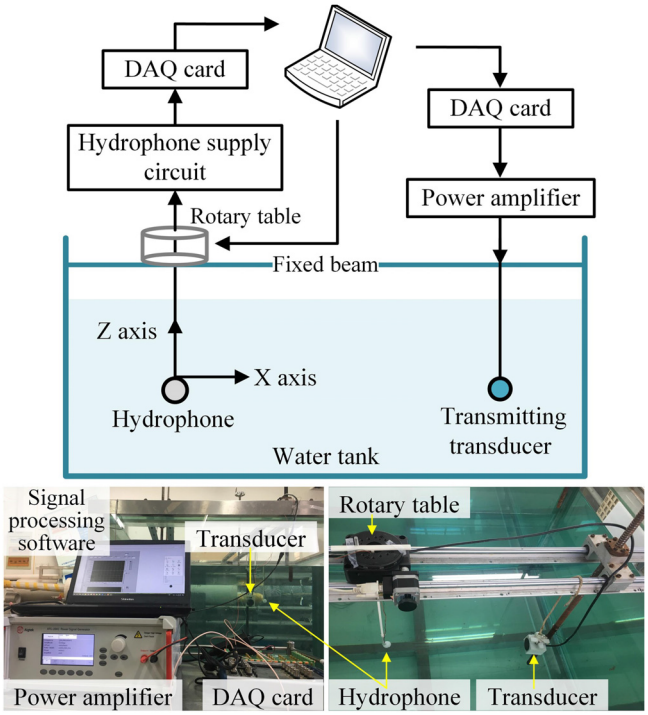

Fig. 4. Performance testing apparatus for the proposed hydrophone.

2-50 Pa which is calculated via dividing the output of the standard hydrophone output by its sensitivity. The computer recorded the output signals of the hydrophone via the acquisition card and calculated the amplitude of received signals with different excitation frequencies, incident directions, and excitation voltages. The hydrophone and the transducer were hanged on a linear guide with the same height and a certain interval distance of 0.4 m. The hydrophone was fixed onto a rotary table, which can be controlled by the computer to rotate around the vertical Z axis to test the hydrophone's directivity. Photosensitive resin (UTR9000) is used for printing material. The model number of the MEMS microphone sealed in the printed shell is SPU0410LR5H-QB; its size is 4 mm × 3 mm × 1.1 mm, its sensitivity is −38 dBV/Pa and its working frequency range is 100 Hz-80 kHz. The power amplifier is Aigtek ATG-2041; it has a max output of ±200 V and work frequency range of DC-500 kHz. Four sets of tests were performed for the proposed hydrophone: frequency response, directivity, sensitivity and SNR, survivability.

A. Frequency Response

Frequency response test was carried out within the frequency range of 5-40 kHz. Because of uneven frequency response of the acoustic emission transducer and the microphone embedded in the hydrophone, the measured frequency response curve was normalized, namely, the curve was divided by the frequency response curves of both the transducer and the microphone. Fig. 5 shows the frequency response curve of the hydrophone with $a = 8$ mm obtained by experiment, which is very close to the result obtained by frequency sweeping simulation. The measured characteristic/ resonance peaks are 14300 Hz, 22600 Hz, and 30800 Hz, which are also very close

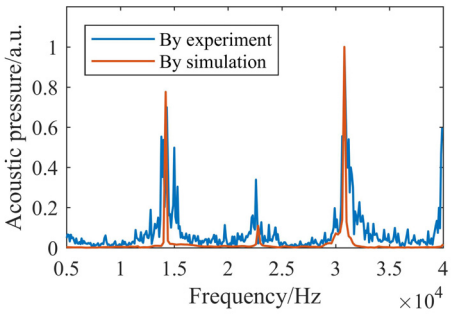

Fig. 5. Frequency response curves obtained by experiment and simulation.

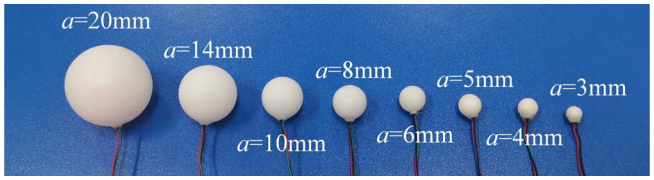

Fig. 6. Air cavity hydrophones with different radii.

to that obtained by simulation as shown in Table I, the second column.

Air cavity hydrophones with different inner radii but with $T = 0.8$ mm were fabricated as shown in Fig. 6, and their frequency response curves were tested. Thereinto, frequency response curves of the hydrophones with the air cavity radii equal to 5 mm, 10 mm and 14 mm are shown in Fig. 7(a)-(c), and the first resonance frequency f_{r1st} of each hydrophone as a function of a is shown in Fig. 7(d). The resonance frequencies obtained by experiments are very close to the modal analysis simulation results. f_{r1st}-a relationship obtained by experiments almost overlaps that obtained by frequency sweeping simulations, which verifies the correctness of the simulation results. At the same time, it can be confirmed again that when a increases, the first-order resonance frequency of the air cavity decreases, and they have an accurate inverse relationship. This demonstrates that the acoustic resonance modes with different frequencies can be precisely predicted, as the inner wall of the solid shell is an acoustically hard boundary and gas-solid coupling does not need to be considered. Peak amplitudes of different characteristic frequencies are quite different. This is because the MEMS microphone is fixed at one point inside the hydrophone, but different frequencies correspond to different acoustic pressure distributions whose max values occur at different locations, as shown in Fig. 3. More than one MEMS microphones can be placed at different positions inside the air cavity to sense different frequencies of sounds, since different frequencies have different acoustic resonance modes.

To find out the relationship between the resonance frequency and the thickness of the shell, several air cavity hydrophones with 8 mm inner radii and various thicknesses ($T = 0.8$ mm, 1.0 mm, 1.5 mm, 2.0 mm, 3.0 mm) were made, as shown in Fig. 8(a). Frequency sweeping experiments were performed using these hydrophones and the frequency response curves of the hydrophones are shown in Fig. 8(b). The peaks indicate

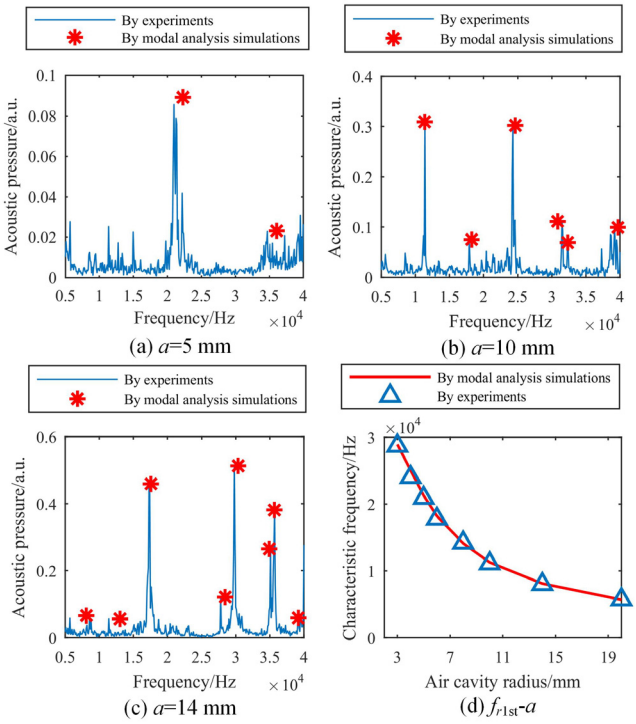

Fig. 7. Frequency responses of air cavity hydrophones with radii of (a) 5 mm, (b) 10 mm, (c) 14 mm; and (d) relationship between the first resonance frequency and air cavity radius by model analysis simulations and experiments.

TABLE II
COMPARISON BETWEEN THE RESONANT FREQUENCY AND THE THICKNESS OF THE SHELL

Thickness (mm)	Resonance frequency (Hz)	Difference from theoretical value
0.8	30900	1.6%
1.0	31200	2.6%
1.5	30900	1.6%
2.0	31100	2.3%
3.0	31200	2.6%
Theoretical value	30396	-

the position of the resonance frequency of the hydrophones, and the accurate frequency values are listed in Table II. The resonance frequencies are not exactly the same as the theoretical value calculated by finite element method simulation, modal analysis of an ideal air sphere; errors may result from temperature variances when sealing assembly or 3D printing roughness that may change a little the ideal, designed air cavity shape. However, it is noticeable that the resonant frequencies are all around 31 kHz regardless of the thickness of the shell, so the resonance frequency of the air cavity is basically irrelevant to the shell thickness.

B. Directivity

Both simulation and experiment were carried out to test the directivity of the hydrophone. The size, thickness and material of the hydrophone shell used in the experiment of directivity test were the same as those used in the simulation. When the microphone was rotated, the incident direction of

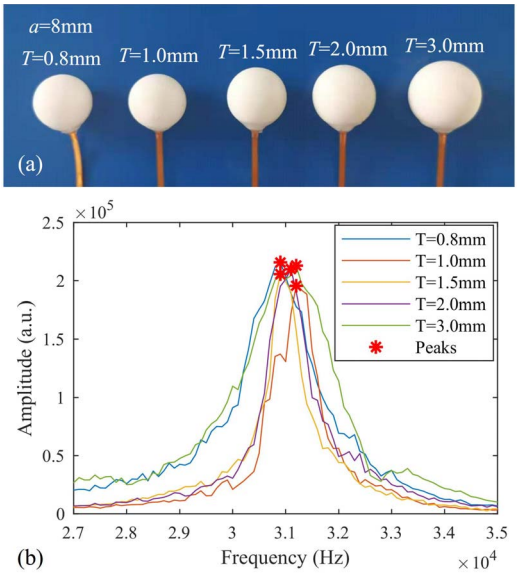

Fig. 8. Frequency response curves of the hydrophones with an identical inner radius and different thicknesses: (a) photo of the tested hydrophone, and (b) frequency response curves of these hydrophones.

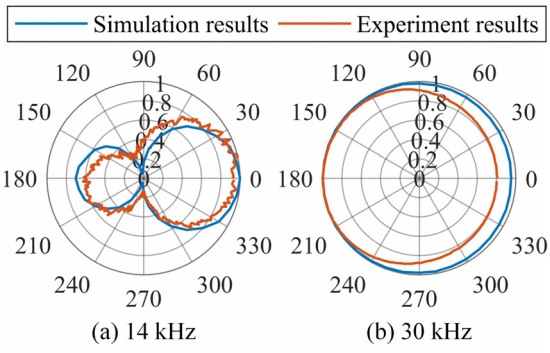

Fig. 9. Normalized directivity in polar coordinate system obtained by simulations and experiments at (a) 14 kHz and (b) 30 kHz.

the acoustic wave was kept unchanged. The simulation was performed in frequency domain, and perfectly matched layers were attached around the water area to eliminate reflection. In the experiment, limited pulse excitation was used and the distance between the transducer and the hydrophone was large enough, so that the direct waves and the echoes can be separated.

When the hydrophone works at different resonance frequencies, the modes of the internal acoustic pressure distribution are different. Taking the hydrophone of $a = 8$ mm as an example, as shown in Fig. 3(a)-(c), for the 30 kHz mode, there is only one small area near the center in the air sphere that has the maximum acoustic pressure; for the 14 kHz mode, there are two areas that have the maximum acoustic pressure and are distributed at the two poles of the air sphere along the incident wave direction. Therefore, when the incident angle of the acoustic wave changes and the microphone is located in the center, for the former mode the hydrophone has no directivity, but for the latter mode it shows a certain directivity. This prediction is verified by simulation and experiment results as shown in Fig. 9.

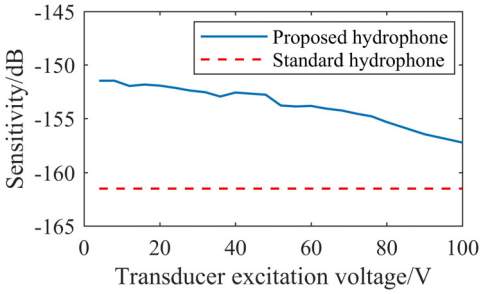

Fig. 10. Sensitivity re 1V/μPa of the proposed hydrophone.

When the incident wave is 30 kHz, during the rotation of the hydrophone, the acoustic pressure measured by simulations changes very little with a fluctuation of about 4.8%; the acoustic pressure measured by experiments also does not significantly change with a fluctuation of about 19.8%. This demonstrates that the hydrophone is basically non-directional at this frequency. When the incident wave is 14 kHz, during the rotation of the hydrophone, the directivity curves measured by simulations and experiments are very similar, and both of them have two obvious poles at the same position. This demonstrates that the hydrophone has obvious directivity at this frequency. Experiments have verified the directivity of the hydrophone at different resonance frequencies and the correctness of the simulation results.

C. Sensitivity and SNR

When testing the sensitivity and SNR of the proposed hydrophone, the emission frequency of the sound source is set to be one of the resonance frequencies. In this experiment of sensitivity and SNR test, the hydrophone with $a = 8$ mm at the resonance frequency of 30 kHz was used. The standard hydrophone (TC4013, Reson) and the newly developed one were placed at the same position to receive the same acoustic pressure. The output voltage of TC4013 and its sensitivity provided by the factory were used to calculate the acoustic pressure at the measuring point. The datasheet reads that when TC4013 is connected to a preamplifier with a gain of 50 dB, its sensitivity is -161 dB re 1V/μPa. Providing U_1 and U_0 are the output voltages of the proposed hydrophone and the standard hydrophone for the same incident sound pressure, respectively, the sensitivity s_A of the proposed hydrophone is calculated as follows: $s_A = 20\log_{10}(U1/U2) - 161$ dB. When the excitation voltage of the transmitting transducer was 4 V to 100 V, the measured sensitivity of the proposed resonant cavity hydrophone was -151 dB to -157 dB re 1V/μPa, as shown in Fig. 10. The test result demonstrates that when the preamplification of the standard hydrophone is 50 dB and the resonant cavity hydrophone has no subsequent amplification, the sensitivity of the latter with a volume of less than 3 cm^3 is higher than that of the former.

The SNRs of the proposed hydrophone and the standard one were calculated by using the simultaneously received underwater acoustic signals at the same measurement point. The SNR is defined as the received signal amplitude of the hydrophone at the resonance frequency when excitation voltage is input into the transducer divided by the amplitude when there is no

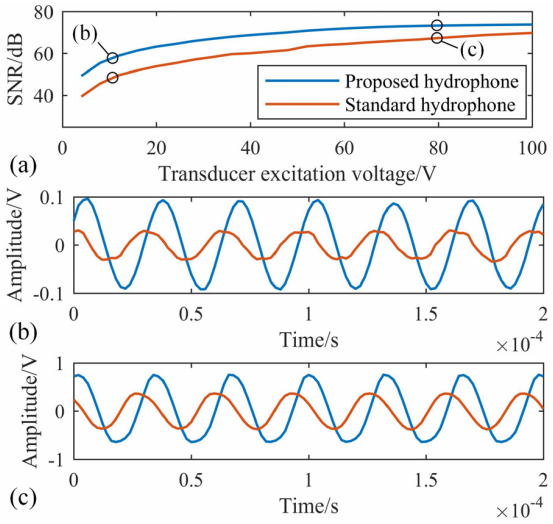

Fig. 11. SNR comparison between the proposed and standard hydrophones: (a) SNR curves of the two hydrophones, (b)-(c) the original signal at the marked points in figure (a).

excitation voltage input into the transducer. As the excitation voltage of the transducer increases, the emitted signal becomes larger and the SNR increases, as shown in Fig. 11(a). The SNR of the proposed hydrophone is greater than that of the standard one. Overall, the difference between the SNRs of the proposed hydrophone and the standard one is small, no more than 10 dB. When the excitation voltages of the transducer are 8 V and 80 V, the original signals in time domain measured by the proposed hydrophone and the standard one are shown in Fig. 11(b)-(c). Both signals are sinusoidal, and the signal amplitude of the proposed resonant cavity hydrophone is larger than that of the standard one. The proposed hydrophone looks distorted at higher levels of transmission because there is an impedance transform amplifier inside the microphone of the proposed hydrophone; when the sound pressure is too high, the amplifier may saturate and will not linearly increase as the transmitted voltage/acoustic pressure continue to increase.

A comparison of the performance of the developed hydrophone based on a resonant air cavity with other reported hydrophones using solid shell and liquid cavity resonances is listed in Table III. The proposed hydrophone is shown to be a competitive and superior performance device compared with the solid and liquid resonance hydrophones. The solid one's resonance frequency is mainly determined by the shape, size and material properties of the solid structures, such as piezoelectric hollow sphere [11] and 1–3 piezoelectric composite [14]. The liquid one's resonance frequency is mainly determined by the shape and size of the liquid cavity formed by a piezoelectric [19] / aluminium [20], [21] / steel [22] tube. Among them, only the hydrophones of [20] and [22] have competitive sensitivities compared with the proposed one. However, they need costly commercial piezoelectric and optic fiber hydrophones to be located in the resonant water-filled tube to form a new hydrophone.

D. Survivability

Survivability is important for a sensor. The long-term survivability test scenario of five hydrophones is shown

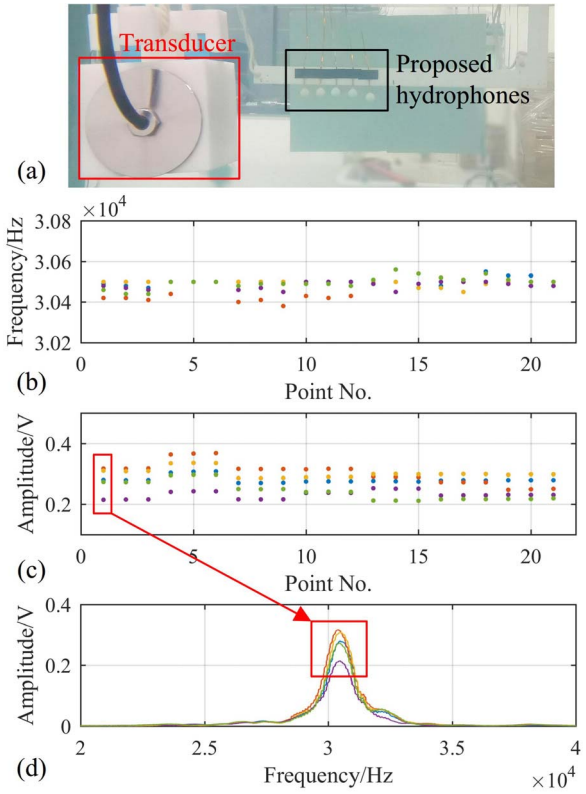

Fig. 12. Long-term survivability test of five hydrophones: (a) photo of test scenario; (b) resonance frequency and (c) amplitude change during two days; (d) frequency response curves of the marked points in figure (c). Different colors represent different hydrophones.

in Fig. 12(a). Several frequency sweeping experiments (20-40 kHz) were carried out to show the change of resonance frequencies and amplitudes at the resonance frequencies as a function of time. The experiments were performed in the morning, afternoon and evening of two different days, and the same experiment was repeated three times. Power supply was given to the hydrophones during the whole days. Besides the frequency-time and the amplitude-time curves as shown in Fig. 12(b)-(c), a frequency response curve at a certain moment is also provided in Fig. 12(d). In fact, the hydrophone can continuously work for several days, and has a stable performance.

IV. Further Discussions

A. Fabrication Cost

One factor needs considering is the fabrication cost. Available manufacturing methods of the proposed hydrophone include 3D printing, mechanical machining, and mold casting. In shallow water applications where the hydrostatic pressure is very small, a plastic shell can be used; therefore, in this scenario 3D printing of the material of photosensitive resin should be used since plastic printing is low cost and the resolution is sufficient. A thin layer of waterproof glue is recommended to be coated onto the surface of the printed spherical shell to increase the waterproof ability when working in the field for a long time. In deep waters or in pressurized liquid-filled pipelines where the hydrostatic

TABLE III
PERFORMANCE COMPARISON OF THE PROPOSED HYDROPHONE WITH OTHER ONES WITH SOLID/LIQUID RESONANT SENSITIZATION STRUCTURES

Hydrophone	Sensing part	Resonance sensitization structures	Sound sensitivity (dB, re: 1 V/μPa)	Resonance frequency
Ref. [11]	Piezoceramic	Piezoelectric hollow sphere	-182 @150 kHz	150 kHz
Ref. [14]	Piezoceramic	1–3 piezoelectric composite	-207.6	975 kHz
Ref. [19]	Piezoceramic	Piezoelectric tube with water inside	-181	5.6 kHz
Ref. [20][21]	Piezoelectric	Aluminum tube with one end open	-165	<2 kHz
Ref. [18]	Piezoresistor	Dumbbell-shaped ciliary	-186.1	1010.8 Hz (in fluid)
Ref. [22]	Optic fiber	Steel tube with two ends closed	-145	1.2 kHz
Ref. [15]	Optic fiber	Microtip and diaphragm	-41.42 dB (re 1 nm/μPa)	4 kHz
Ref. [16]	Optic fiber	Rigid tube, cylindrical mandrel and two optical fiber coils	-140	1.6 kHz
Ref. [17]	Optic fiber	Optical ring resonator	Not mentioned	3 MHz~6 MHz
Ref. [3]	MEMS microphone	Mo-AlN-Mo piezoelectric stack	-180	10 Hz to 8 kHz
This work	MEMS microphone	Air cavity	-157 @30 kHz	$fr \propto a$, <40 kHz

pressure is very high, a ruggedized metal shell should be used. In this case, mechanical machining and mold casting should be used, and alternative materials include aluminum, stainless steel, and titanium alloys. Since the sensor is already packaged/assembled and the signal is already conditioned, a lot of tedious steps have been saved, so the fabrication of the proposed hydrophone is low cost.

B. Temperature

Another factor needs considering is temperature change that may slightly lower the sensitivity of the proposed hydrophone. Since temperature and pressure have a definite mathematical relationship determined by the equation of gas state, only temperature needs to be considered. The speed of sound c_0 in m/s in air has an approximately linear relationship with the temperature t_0 in °: $c_0 = 331.4 + 0.607 \times t_0$ [29]. The resonance frequency of the air cavity is proportional to the speed of sound c_0 according to (5). When the ambient temperature changes from 10° to 20°, for instance, c_0 changes by 1.8% (6.07/337.47), so the resonance frequency also changes by 1.8%. Therefore, the sensitivity of the proposed hydrophone will go down since the resonance frequency deviates from the designed value as the ambient temperature changes. At lower resonance frequencies with smaller absolute frequency shifts, sensitivities are reduced less because the bandwidths of different modes are almost the same, as can been seen from the frequency response test results as shown in Fig. 5 and Fig. 7.

C. Longevity

Longevity needs to be considered for a long-term use in the field. The service life of the proposed hydrophone depends on the structural stability and the sealing performance of the joint. Spherical shell, T-shaped plug, and small wire hole have already been used by the proposed hydrophone to increase its structural stability. In the principle verification stage, UV glue is used, because UV glue is cured via ultraviolet irradiation, so it is clean and convenient. In the final product, epoxy resin is recommended for sealing the T-shaped plug and the small wire hole. It is recommended to seal the shell in dry air or probably nitrogen to avoid condensation at low temperatures and to ensure longevity. However, the speed of sound is affected with a very small extent by the humidity [30]. For example, at 298K (25°) when the relative humidity changes from 10% to 90%, the speed of sound changes by about 0.3%(1/347) and the resonance frequency also changes by 0.3% that is much less than the band relative to the resonance frequency obtained via experiments.

D. Narrow Bandwidth

The proposed hydrophone is narrowband, so it cannot satisfy all kinds of applications. However, an important application of the narrow bandwidth hydrophone is the ultra-short base line (USBL) positioning technology. USBL positioning technology is widely used in both civil and military fields. In the civil area, underwater surveys, marine surveys, diver operations, underwater salvage, underwater engineering, etc. all require the support of hydroacoustic positioning; the military area includes frogman activities, submarine navigation, AUV recovery, deep-sea exploration, coordination positioning, enemy ship detection and other applications. In the USBL system, the detected target emits a single-frequency underwater acoustic signal, and the shipborne hydrophone array receives the single-frequency signal and uses the phase difference of the multiple signals to calculate the azimuth and distance of the target.

Another important application of the narrow bandwidth hydrophone is leak detection of oil/water transportation pipelines. The original leak sound signal is broadband no matter how large the pipe diameter is and how large the leak hole is, so the acoustically resonant, narrow-band hydrophone can always capture the leak signal. The hydrophone shell forms a closed air cavity which may acoustically resonate and thus amplify the transmitted sound induced by leaks. The resonant cavity hydrophone may have very high leak detection sensitivity but low cost. It can be widely used in leak detection of water supply pipe network.

E. Bandwidth Broadening

A wider bandwidth is certainly more flexible in use. To broaden the bandwidth, a possible way was tried out, that is, arranging several air cavities of continuously increasing radii in a line and sealing several microphones inside each

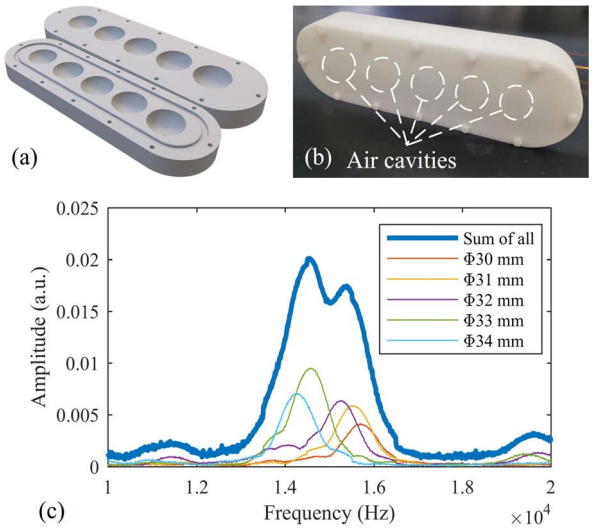

Fig. 13. Multi-cavity hydrophone: (a) 3D model and (b) photo of the structure; (c) frequency response curves of each cavity and the sum of all channels.

cavity to simultaneously acquire the signals and add up the signals. In this way, the bandwidth can be broadened to a certain extent. To demonstrate this, a structure with multiple cavities shown in Fig. 13(a)-(b) was fabricated via 3D printing, and some test experiments were carried out.

Two semi-cavities are printed separately, one of which has an O-ring groove and five wire holes. Microphones are inserted into the cavities through these small holes and then fixed with UV glue. A rubber O-ring is put into the groove, and the two parts are closed facing each other and then clamped with screws to achieve sealing. When these two parts are assembled, five spherical air cavities are formed. The diameters of five cavities are designed to be 30 mm, 31 mm, 32 mm, 33 mm, and 34 mm, respectively. The resonance frequencies calculated by FEM simulations, acoustic modal analyses are 16364 Hz, 15836 Hz, 15341 Hz, 14877 Hz, and 14439 Hz. Frequency sweeping experiments were performed to test the frequency response of the multi-cavity hydrophone. The results are shown in Fig. 13(c). The resonance frequency of the cavities may not be exactly the same as the theoretical value, due to the 3D printing roughness and assembly error that may destroy the ideal, designed air cavity shape. The five curves were added up, and finally a wider broadband compared with a single hydrophone is obtained.

V. Conclusion

This paper demonstrates a low-cost, high-sensitivity hydrophone based on a resonant air cavity. The hydrophone consists of a thin solid shell containing an air cavity and a tiny affordable MEMS microphone that is sealed inside to sense the focused acoustic waves transmitted from the external water across the shell into the air cavity without destroying the acoustic field distribution mode inside. Both finite element simulations and experiments are carried out to test its acoustic sensing performances. The resonance frequency of the proposed hydrophone is determined by the radius of the air cavity and the acoustic mode, but is independent of the solid shell, which facilitates the precise designability. Different modes of internal acoustic field distributions lead to different directivities. The sensitivity and SNR of the hydrophone at the resonance frequency are higher than those of the commercial standard one, when the former with a volume less than 3 cm^3 has no subsequent amplification and the latter is connected with a 50 dB amplifier in series. Its sensitivity is up to -151 dB re 1V/μPa. Finally, several further considerations and applications on the proposed hydrophone are discussed.

References

[1] X. Mo, "Progress and opportunities of underwater transducers in China," *Bull. Chin. Acad. Sci.*, vol. 34, no. 3, pp. 272–282, 2019.
[2] J. Weng and Y. Yang, "A passive source range and depth estimation method by single hydrophone in shadow zone of deep water," *Acta Acustica*, vol. 43, no. 6, pp. 905–914, Nov. 2018.
[3] J. Xu *et al.*, "Low-cost, tiny-sized MEMS hydrophone sensor for water pipeline leak detection," *IEEE Trans. Ind. Electron.*, vol. 66, no. 8, pp. 6374–6382, Aug. 2019.
[4] E. M. Fischell, A. R. Kroo, and B. W. O'Neill, "Single-hydrophone low-cost underwater vehicle swarming," *IEEE Robot. Autom. Lett.*, vol. 5, no. 2, pp. 354–361, Apr. 2020.
[5] T. Necsoiu, I. Chilibon, M. Robu, V. Cătuneanu, and A. Stan, "Some aspects of the piezoceramic materials utilized in sensitive hydrophones," *Sens. Actuators A, Phys.*, vol. 60, nos. 1–3, pp. 139–141, May 1997.
[6] J. A. Brown, K. Dunphy, J. Leadbetter, B. A. Rob, and O. Beslin, "A single-crystal acoustic hydrophone for increased sensitivity," presented at the 21st Int. Congr. Acoust., Montreal, QC, Canada, Jun. 2013.
[7] Q. Jing and X.-J. Li, "Preparation of porous barium titanate ceramics and enhancement of piezoelectric sensitivity," *Acta Phys. Sinica*, vol. 68, no. 5, 2019, Art. no. 057701.
[8] S. Sebastion, S. Sridhar, P. S. Prasad, and S. Asokan, "Highly sensitive fiber Bragg grating-based pressure sensor using side-hole packaging," *Appl. Opt.*, vol. 58, no. 1, pp. 115–121, Jan. 2019.
[9] A. I. Azmi, D. Sen, and G.-D. Peng, "Sensitivity enhancement in composite cavity fiber laser hydrophone," *J. Lightw. Technol.*, vol. 28, no. 12, pp. 1844–1850, Jun. 15, 2010.
[10] C. Li, X. Peng, J. Liu, C. Wang, S. Fan, and S. Cao, "D-shaped fiber Bragg grating ultrasonic hydrophone with enhanced sensitivity and bandwidth," *J. Lightw. Technol.*, vol. 37, no. 9, pp. 2100–2108, May 1, 2019.
[11] D. Teng, H. Yang, and G. Zhu, "Design and test about high sensitivity thin shell piezoelectric hollow sphere hydrophone," presented at the Oceans, Anchorage, AK, USA, Sep. 2017.
[12] S. Sadeghpour, S. Meyers, J.-P. Kruth, J. Vleugels, M. Kraft, and R. Puers, "Resonating shell: A spherical-omnidirectional ultrasound transducer for underwater sensor networks," *Sensors*, vol. 19, no. 4, p. 757, Feb. 2019.
[13] W. Wang, J. Wu, X. Luo, L. Zhou, X. Xu, and Q. Ma, "Jump effect based magnetically tunable resonance of PZT-ring/TDF-strip composite with improved sensitivity," *Sens. Actuators A, Phys.*, vol. 225, pp. 47–52, Apr. 2015.
[14] Z. Yang, H. Wang, D. Zeng, C. Zhao, and Z. Chen, "Dynamic modeling of 1–3 piezoelectric composite hydrophone and its experimental validation," *Composite Struct.*, vol. 150, pp. 246–254, Aug. 2016.
[15] S. Dass, S. Kachhap, and R. Jha, "Hearing the sounds of aquatic life using optical fiber microtip-based hydrophone," *IEEE Trans. Instrum. Meas.*, vol. 69, no. 7, pp. 4015–4020, Jul. 2020.
[16] C. Peng, X. Zhang, and Z. Meng, "Bearing estimation for optical fiber vector hydrophone with in-band resonance," *Appl. Acoust.*, vol. 158, Jan. 2020, Art. no. 107055.
[17] H. Chen, Z. Shao, Y. Hao, and Q. Rong, "A high-frequency hydrophone using an optical fiber microknot resonator," *Opt. Commun.*, vol. 446, pp. 77–83, Sep. 2019.
[18] S. Ji *et al.*, "Design and realization of dumbbell-shaped ciliary MEMS vector hydrophone," *Sens. Actuators A, Phys.*, vol. 311, Aug. 2020, Art. no. 112019.
[19] S. P. Li, X. P. Mo, and Y. Z. Pan, "A high sensitivity piezoelectric ceramic hydrophone with coupling fluid cavity," *Acta Acustica*, vol. 42, no. 6, pp. 729–736, 2017.

[20] Z. F. Wang, Y. M. Hu, Z. Meng, and M. Ni, "Acoustic characteristics of underwater cylindrical Helmholtz resonator," *Acta Phys. Sinica*, vol. 57, no. 11, pp. 7022–7029, Nov. 2008.
[21] Z. F. Wang, Y. M. Hu, H. Luo, Z. Meng, M. Ni, and S. Xiong, "Influence of cavity wall elasticity on resonant frequency of small underwater cylindrical Helmholtz resonator," *Acta Phys. Sinica*, vol. 58, no. 4, pp. 2507–2512, Apr. 2009.
[22] Z. Wang, Y. Hu, Z. Meng, and M. Ni, "Fiber-optic hydrophone using a cylindrical Helmholtz resonator as a mechanical anti-aliasing filter," *Opt. Lett.*, vol. 33, no. 1, pp. 37–39, Jan. 2008.
[23] M. A. Shah, I. A. Shah, D. G. Lee, and S. Hur, "Design approaches of MEMS microphones for enhanced performance," *J. Sensors*, vol. 2019, Mar. 2019, Art. no. 9294528.
[24] S. A. Zawawi, A. A. Hamzah, B. Y. Majlis, and F. Mohd-Yasin, "A review of MEMS capacitive microphones," *Micromachines*, vol. 11, no. 5, p. 484, May 2020.
[25] S. Dass and R. Jha, "Tapered fiber attached nitrile diaphragm-based acoustic sensor," *J. Lightw. Technol.*, vol. 35, no. 24, pp. 5411–5417, Dec. 15, 2017.
[26] S. Dass and R. Jha, "Micro-tip cantilever as low frequency microphone," *Sci. Rep.*, vol. 8, no. 1, Aug. 2018, Art. no. 012701.
[27] S. Dass, S. Kachhap, and R. Jha, "S-shaped microfiber based diaphragm supported optical microphone," *J. Phys., Photon.*, vol. 1, no. 2, May 2019, Art. no. 025005.
[28] J. Cheng, *Principles of Acoustics*. Beijing, China: Science Press, 2012, pp. 411–439.
[29] L. L. Beranek, *Acoustics*. Cambridge, MA, USA: The Acoustical Society of America, 1993, p. 10.
[30] T. Motegi, K. Mizutani, and N. Wakatsuki, "Simultaneous measurement of air temperature and humidity based on sound velocity and attenuation using ultrasonic probe," *Jpn. J. Appl. Phys.*, vol. 52, no. 7S, Jul. 2013, Art. no. 07HC05.

Huang Xinjing received the B.S. and Ph.D. degrees from Tianjin University, in 2010 and 2016, respectively. He is currently an Associate Professor with Tianjin University. His research interests include structural health monitoring and damage detection for underwater infrastructure with acoustic and/or magnetic methods.

Li Zan received the B.E. degree from Tianjin University, in 2019, where he is currently pursuing the master's degree with the Instrument Science and Technology Department. His research interests include acoustic sensors and metamaterials.

Li Jian received the B.E., M.E., and Ph.D. degrees from Tianjin University, in 1994, 1997, and 2000, respectively. He is currently a Professor with Tianjin University. His research interests include pipeline leak detection and pipeline safety warning with acoustic methods.

Wang Xin, photograph and biography not available at the time of publication.

Feng Hao, photograph and biography not available at the time of publication.

Zhang Yu, photograph and biography not available at the time of publication.

Rui Xiaobo, photograph and biography not available at the time of publication.